nature communications

Article

https://doi.org/10.1038/s41467-025-67429-6

The visual system of the longest-living vertebrate, the Greenland shark

Received: 2 July 2025

Accepted: 27 November 2025

Published online: 05 January 2026

Check for updates

Lily G. Fogg[1], Emily Tom[2,3], Maxime Policarpo[1,4], William Cho[3], Fangyuan Gao[2], Doreen Hii[5], Aaron E. Fawcett[5], Nicolas Boileau[1], Amalie Bech-Poulsen[6], Kirstine F. Steffensen[6], Cherlyn J. Ng[5], Peter G. Bushnell[7], John Fleng Steffensen[6,9], Richard Brill[8], Walter Salzburger[1,10] & Dorota Skowronska-Krawczyk[2,3,10]

The Greenland shark (*Somniosus microcephalus*) is the longest-living vertebrate and inhabits the exceptionally dim and cold waters of the Arctic deep sea. Due to its extreme lifespan, harsh environmental conditions, and prevalent corneal parasitisation, the Greenland shark has previously been thought to have impaired or degenerated vision. Here, we present genomic, transcriptomic, histological and functional evidence that the Greenland shark retains an intact visual system well-adapted for life in dim light. Histology and in vitro opsin expression revealed visual adaptations typical of deep-sea species, including densely packed, elongated rods and a short-wavelength shift in rod visual pigment sensitivity compared to shallow-water sharks. In situ hybridisation confirmed the presence of essential visual cell types: rods, Müller glia, and bipolar, amacrine, and ganglion cells. Moreover, despite being over a century old, the examined specimens showed no obvious signs of retinal degeneration. Using whole genome and retinal RNA-sequencing, we further show that dim-light (rod-based) vision genes are intact and robustly expressed, while many bright-light (cone-based) vision genes have become pseudogenized and/or are no longer expressed. Finally, we identify robust expression of DNA repair-associated genes in the retina, which may help support long-term maintenance of retinal integrity over the Greenland shark's extreme lifespan.

The Greenland shark (*Somniosus microcephalus* [Bloch & Schneider 1801][1]; Fig. 1a; Fig. S1) is the longest-living vertebrate on Earth, with an estimated lifespan of up to 400 years[2]. This deep-sea shark inhabits regions from the temperate North Atlantic to the frigid waters of the Arctic Ocean, enduring temperatures as low as −1.1 °C and depths approaching 3000 meters[3–5]. In the waters surrounding Greenland, their eyes are frequently parasitized by copepods (*Ommatokoita elongata*), which are thought to obscure vision by attaching to the cornea[6–9]. Despite their slow-moving nature, Greenland sharks are opportunistic feeders, consuming a range of prey, from fish and squid

[1]Zoological Institute, Department of Environment Sciences, University of Basel, Basel, Switzerland. [2]Gavin Herbert Eye Institute, Brunson Center for Translational Vision Research, Department of Ophthalmology and Visual Sciences, University of California, Irvine, CA, USA. [3]Department of Physiology and Biophysics, University of California, Irvine, CA, USA. [4]Evolution of Sensory and Physiological Systems, Max Planck Institute for Biological Intelligence, Martinsried, Germany. [5]Department of Cognitive Sciences, School of Social Sciences, University of California Irvine. 3151 Social Sciences Plaza, Irvine, CA, USA. [6]University of Copenhagen, Marine Biological Section, Department of Biology, Helsingør, Denmark. [7]Department of Biological Sciences, Indiana University South Bend, South Bend, IN, USA. [8]Virginia Institute of Marine Science, Gloucester Point, VA, USA. [9]Deceased: John Fleng Steffensen. [10]These authors contributed equally: Walter Salzburger, Dorota Skowronska-Krawczyk. e-mail: lily.fogg@unibas.ch; walter.salzburger@unibas.ch; dorotask@hs.uci.edu

https://doi.org/10.1038/s41467-025-67429-6

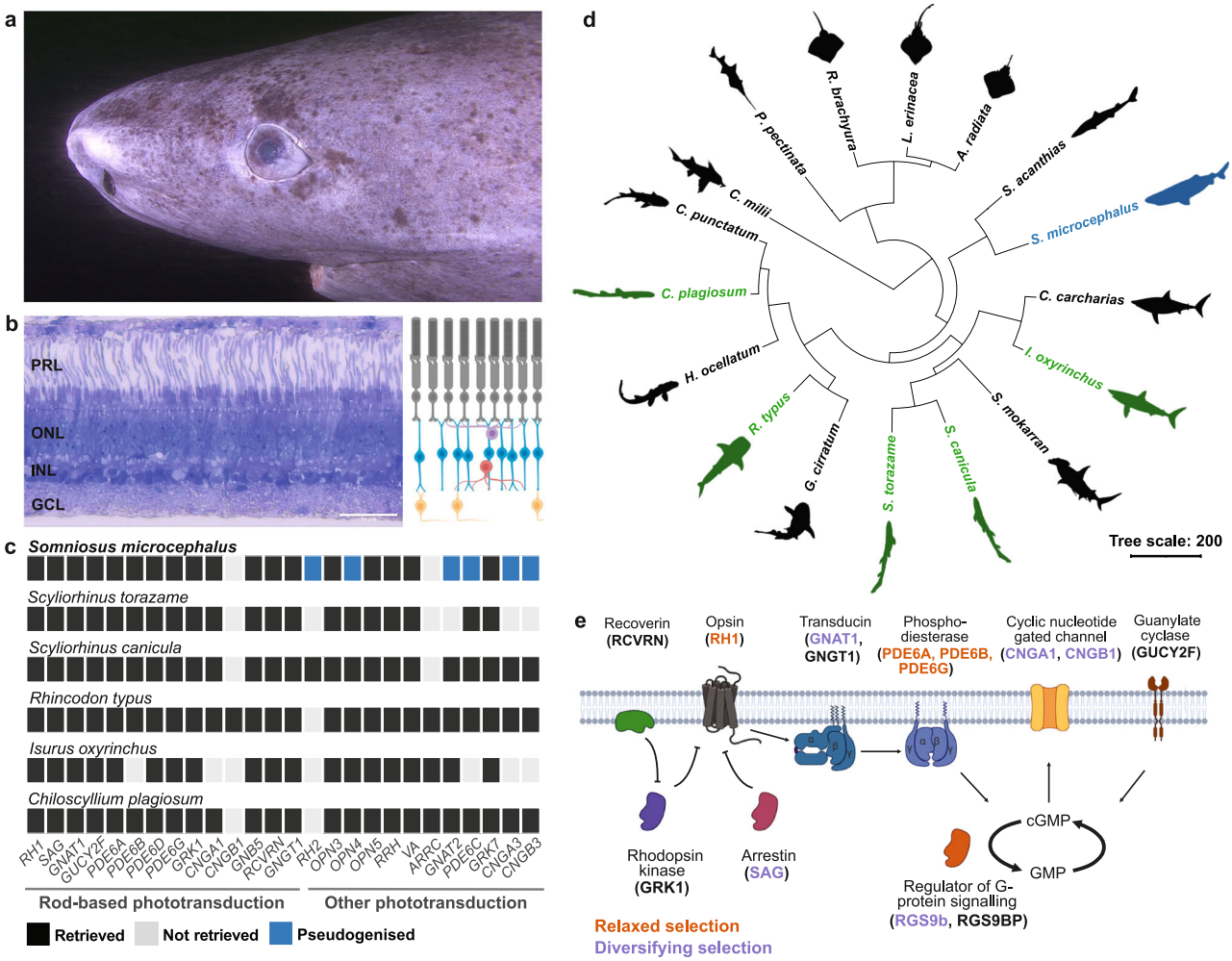

Fig. 1 | Visual system of the Greenland shark. a Representative photograph of the head and eye of a Greenland shark, *Somniosus microcephalus*. **b** Transverse section through the retina of the Greenland shark ($n = 1$ individual), alongside schematic illustration of the retinal layers. ***Scale bar:*** 50 μm. **c** Tile plot summarising phototransduction gene mining. Note that most sharks (including the Greenland shark) lack a copy of *cngb1*. **d** Species tree showing phylogenetic placement of the Greenland shark (blue), and five comparison species (green; *Scyliorhinus canicula, S. torazame, Isurus oxyrinchus, Rhincodon typus*, and *Chiloscyllium plagiosum*) used in this study, within the class, Chondrichthyes. Scale is in million years. **e** Schematic of the components of the rod-based phototransduction cascade found in the genome of the Greenland shark, with gene names coloured by evidence for relaxed (orange) or diversifying (purple) selection. ***Abbreviations:*** PRL, photoreceptor layer; ONL, outer nuclear layer; INL, inner nuclear layer; GCL, ganglion cell layer. Photograph in panel a was provided with permission for use by Ghislain Bardout from the Under the Pole expedition. Panel **e** was created using BioRender [Fogg, L. (2025) https://BioRender.com/ybje926]. Source data are provided as a Source Data file.

to seals and large carrion, such as whale carcasses[3,5,10]. The unique combination of extreme longevity, persistent low temperatures, high-pressure conditions, and parasitised eyes presents unparalleled challenges for its ability to see – raising fundamental questions about the nature and function of the visual sensory system in this enigmatic species.

Vertebrate visual systems have evolved across diverse photic environments, from bright terrestrial habitats to the perpetual darkness of caves and the deep sea. In most vertebrate species, vision relies on two types of retinal photoreceptors: rods, optimized for low-light (scotopic) vision, and cones, specialized for bright-light (photopic) vision[11]. Rods are highly sensitive, with abundant chromatophore-bound visual pigments (opsins) and an efficient phototransduction cascade, while cones provide saturation-resistant, broad-spectrum photic sensitivity[12]. The relative proportion of rods and cones and the spectral tuning of their opsins are primarily shaped by ecological pressures[13–21]. While rod visual pigments (based on the RH1 opsin) are typically maximally sensitive to blue-green wavelengths (460–530 nm), cone visual pigments (SWS1, SWS2, RH2, and LWS) span a broader range of peak sensitivities, from ultraviolet to red light (350–600 nm)[22]. Deep-sea and nocturnal species often exhibit rod-dominated retinas, sometimes to the complete exclusion of cones, as in certain nocturnal reptiles[23], deep-sea teleost fishes[24] and deep-sea sharks[25–29].

In the most extreme conditions, vision can be entirely lost. Cavefishes, for instance, have evolved in complete darkness, leading to retinal degeneration, loss of phototransduction gene expression, and widespread pseudogenization of vision-related genes[30–32]. Given the Greenland shark's exceptionally dim and potentially obstructed visual environment in combination with its extreme longevity, it has been speculated that it, too, may have lost its ability to see[5,8,33]. However, behavioural observations suggest that these sharks may still rely on sight[34], and their optic tectum—a brain region that processes visual information—is comparable in size to that of other visually capable elasmobranchs[35]. Furthermore, the Greenland shark has a tapetum lucidum, a specialized reflective layer behind the retina that enhances photon capture in low-light conditions[36].

In this study, to determine whether the Greenland shark possesses a lifelong functional visual system, we conducted a comprehensive

integrative analysis incorporating genomics, transcriptomics, in situ hybridisation (RNAscope), ultramicrotomy, chromatin staining, mass spectrometry, in vitro opsin regeneration, and spectrophotometry. Our findings support the presence of a preserved and functional visual system in the adult Greenland shark, which seems well-adapted to extreme low-light conditions. Additionally, transcriptomic data suggest a role for DNA repair mechanisms in maintaining retinal integrity over centuries, potentially contributing to the longevity of vision in the longest-living vertebrate.

Results and Discussion

Structural and genomic basis of vision in the Greenland shark

Vertebrates typically possess a duplex retina containing both rods and cones. Many deep-sea fish species feature rod-dominated or even pure-rod retinas to enhance scotopic vision[13,28]. Using histology, we show that the Greenland shark retina also exhibits a pure-rod structure. In addition, the retina displays several morphological features associated with dim-light adaptation, including densely packed and elongated rods, and comparatively thin inner retinal layers (Fig. 1b), resembling those of other deep-dwelling or nocturnal sharks[28,37,38]. All retinal layers are intact in the Greenland shark, including the photoreceptor layer, the outer nuclear layer, the inner nuclear layer, and the ganglion cell layer (Fig. 1b, Fig. S45–S46). That is, even though the retinas inspected were from adult Greenland sharks estimated to be over a century old, there were no obvious signs of retinal degeneration.

To further assess whether the Greenland shark retina shows signs of age-related degeneration, we performed a TUNEL (Terminal deoxynucleotidyl transferase dUTP Nick End Labeling) assay on cryosections of the retina. This assay detects DNA fragmentation, a hallmark of apoptosis and other forms of cell death often associated with degenerative processes in vertebrates[39–42]. As a positive control, sections were treated with DNase I to induce DNA breaks, which produced a robust TUNEL signal as expected, confirming the assay's sensitivity and functionality. In contrast, no TUNEL-positive cells were observed in the untreated retinal sections from the Greenland shark (Fig. 2e). This absence of detectable DNA fragmentation suggests there is no ongoing DNA damage and cell death within the retina.

The absence of obvious signs of retinal degeneration is remarkable given that even in healthy aging, vertebrate retinas (including those of humans) undergo progressive photoreceptor loss and DNA damage over time[40]. For example, at published rates of age-related rod loss (approximately 0.2–0.6% per year), a human living to 400 years of age would be expected to lose over 50–90% of their rod photoreceptors[43–45]. Although it is worth noting that metabolic temperature effects may attenuate rates of cellular decline in cold-water species, such as the Greenland shark. Systematic studies of retinal aging in other long-lived species remain scarce. However, existing data suggest that elephants retain stable photoreceptor populations with age[46], and turtles and tortoises can exhibit slow or negligible senescence (though the retina itself was not examined in this group)[47]. The oldest Greenland shark specimen analysed here was estimated to exceed 130 years of age – making it two- to four-fold older than the eldest individuals examined in elephants, turtles and tortoises. Thus, the Greenland shark provides a striking example of long-term preservation of retinal integrity, supported at both molecular and histological levels, and highlights the extraordinary potential for neuronal maintenance in extreme longevity.

Vertebrate photoreception relies on a cascade of biochemical reactions mediated by numerous phototransduction genes, many of which are specialised for either rods, cones, or non-visual photoreceptive cells, such as intrinsically photosensitive retinal ganglion cells (ipRGCs)[12,48]. Deep-dwelling fish species typically rely more on scotopic vision and, hence, the rod-specific phototransduction genes[16,49,50]. To examine the phototransduction gene repertoire of the Greenland shark, we generated a draft genome for this species and screened it for phototransduction genes. We retrieved functional copies for the full complement of genes required for rod-based phototransduction (Fig. 1c), including *rh1, sag, gnat1, gucy2f, pde6a, pde6b, pde6d, pde6g, grk1, cnga1, gnb5, rcvrn* and *gngt1*. The same set of rod-specific phototransduction genes was found in the genomes of five other shark species (*Scyliorhinus canicula, S. torazame, Isurus oxyrinchus, Rhincodon typus*, and *Chiloscyllium plagiosum*; Fig. 1c; Fig. S2), which typically inhabit the upper pelagic zone of tropical to warm temperate seas[51–55]. Unlike in the other shark genomes inspected, only one gene typically associated with cone phototransduction (*grk7*) was retrieved from the Greenland shark genome, and recent evidence suggests *grk7* may also function in rods in some elasmobranchs[56]. The remaining cone-associated phototransduction genes present in the other sharks were either not found in our draft genome (*arrc*) or were pseudogenized (*rh2, gnat2, pde6c, cnga3*, and *cngb3*) (Fig. 1c). This suggests that Greenland sharks rely on rod-based vision, just like another deep-dwelling shark, the lanternshark *Etmopterus spinax*[25] and many deep-sea teleosts[13].

We further found that the Greenland shark has a single functional copy of the visual opsin gene *rh1*, and the non-visual opsins *opn3, opn5, rrh* and *va*—a pattern similar to that of other sharks[29,57]. Like several other shark species[58], the Greenland shark lacks a functional copy of the green-sensitive cone opsin gene (*rh2*), and this gene also shows signs of pseudogenization in the Greenland shark's genome. Unique among sharks—but similar to what has happened in some cavefish species[30]—is the pseudogenization of the non-visual opsin gene *opn4* in the Greenland shark. In mammals, *opn4* encodes melanopsin, a photopigment expressed in intrinsically photosensitive retinal ganglion cells (ipRGCs) that contribute to non-image-forming light responses, including circadian photoentrainment[59,60]. However, in dim-light environments, such as the deep sea, rods and cones are primarily responsible for circadian entrainment[61], potentially reducing the functional importance of melanopsin-based pathways. The loss of *opn4* in the Greenland shark may thus reflect an adaptation to its deep-sea habitat. Supporting this idea, Greenland sharks do not exhibit a clear circadian rhythm in their diel vertical movement patterns[33,62].

Finally, by computing the ω ratio (*i.e.*, dN/dS) and conducting selection tests, we found that some of the rod-specific phototransduction genes, including *rh1*, showed evidence of relaxed selection relative to other sharks, suggesting that they are under less pressure to be maintained in the Greenland shark genome compared to other species (Fig. 1e; Fig. S13–S43). However, no loss-of-function mutations were detected in this pathway, which would be expected if they were in the process of being pseudogenized[30]. Furthermore, some rod genes (*e.g., gnat1* and *sag*) showed evidence of diversifying positive selection, which may suggest adaptive changes related to the optimisation of rod-based vision in the Greenland shark.

Subcellular adaptations and circuitry of the Greenland shark retina

To investigate whether the retinal tissue of the Greenland shark actively maintains nuclear organization, which is indicative of active transcription and hence cellular metabolism, we assessed the presence of histone modifications associated with active (H3K27Ac) and repressive (H4K20me3) chromatin states[63]. We found clear signals for both histone markers in all nuclear layers of the retina (Fig. 2a), indicating active maintenance of chromatin structure across all cell types. Notably, in rod cells, the active H3K27Ac marker was primarily localized to the centre of the nucleus, while the repressive H4K20me3 marker was predominantly found near the nuclear lamina (Figs. 2b, c). This nuclear organization pattern has previously been associated with diurnality (and therefore, being active in bright light) in mammals[64]. That we now also found this pattern in an elasmobranch species that is predominantly active in dim light suggests that associations between

https://doi.org/10.1038/s41467-025-67429-6

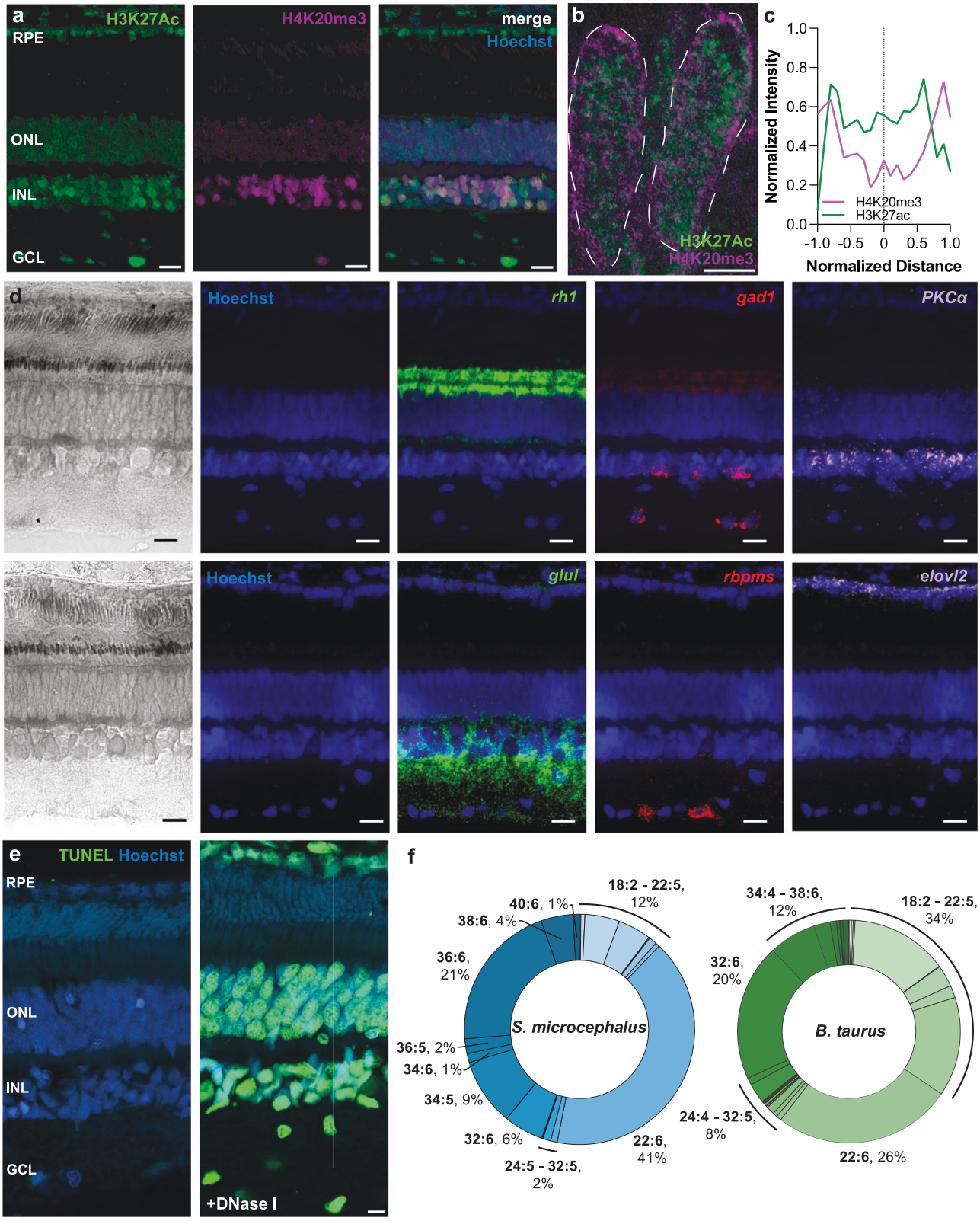

nuclear architecture and diel activity may differ across lineages and ecological contexts. Overall, the presence of both active and repressive chromatin states suggests that the retina of the Greenland shark is indeed metabolically and transcriptionally active.

To assess the integrity of the visual circuit, we employed cell-type specific probes in fluorescent RNA in situ hybridization (RNAscope) to target specific retinal cell types, including rods (using a probe for *rh1*), GABAergic amacrine cells (*gad1*), rod bipolar cells (*pkcα*), Müller glia (*glul*), retinal ganglion cells (*rbpms*) and glycinergic amacrine cells (*slc6a9*)[65,66]. Using this approach, we confirmed the presence of all key cell populations necessary for rod-based vision, confirming the integrity of the retinal circuitry in the Greenland shark (Fig. 2d).

Next, we examined the polyunsaturated fatty acid (PUFA) composition of the Greenland shark retina, with a particular focus on

Fig. 2 | Intact visual circuit and subcellular visual adaptations in the Greenland shark. a Immunofluorescent staining of retinal cross-sections from the Greenland shark labelling active (H3K27Ac) and repressed (H4K20me3) chromatin, counter-stained with Hoechst. **b** Higher magnification image of H4K20me3 and H3K27Ac localization in photoreceptor nuclei ($n = 1$ individual). Dashed white line demarcates the nuclear membrane. **c** Distribution of H4K20me3 and H3K27Ac immunofluorescent signal intensity in the nucleus. Dashed line indicates the center of the nucleus. **d** In situ hybridisation of key retinal cell markers in retinal cross-sections ($n = 1$). Note that the expression of *elovl2*, a key gene in synthesis of VLC-PUFAs, is confined to the retinal pigment epithelium cells in the Greenland shark, in contrast to previous work showing zebrafish expression in Müller glia[71] and human expression in cones[67]. **e** In situ DNA fragmentation detected by TUNEL staining in retinal cross-sections from the Greenland shark ($n = 1$). DNase I treatment was used as a positive control. **f** PUFA composition of bovine ($n = 5$) and Greenland shark retinas ($n = 2$) showing the relative abundance of each PUFA, normalized to the total signal intensity of all detected PUFAs by liquid chromatography-mass spectrometry (LC-MS). Since LC-MS cannot reliably distinguish between omega-3 and omega-6 species, we have reported only the total number of carbon atoms and double bonds for each lipid species in the panels. Brackets highlight the most abundant sets of PUFAs in each animal's retina, allowing for a straightforward visual comparison of the relative abundance of specific fatty acids. ***Scale bars:*** 25 μm **(a, d)**, 5 μm (**b**), 10 μm (**e**). ***Abbreviations:*** RPE, retinal pigment epithelium; ONL, outer nuclear layer; INL, inner nuclear layer; GCL, ganglion cell layer. Source data are provided as a Source Data file.

omega-3 docosahexaenoic acid (DHA, 22:6n-3) and very-long-chain polyunsaturated fatty acids (VLC-PUFAs) containing 24 or more carbon atoms. These lipids support rhodopsin function via membrane fluidity and pigment packing[67–69] and have been associated with counteracting cold-induced membrane rigidity[70]. First, we noted that *elovl2*, a key gene in synthesis of VLC-PUFAs in zebrafish[71] and humans[67], is expressed in the Greenland shark retina, specifically in the retinal pigment epithelium (RPE) cells (Fig. 2d). Liquid chromatography-mass spectrometry (LC-MS) analysis revealed that the retina of the Greenland shark contains an exceptionally high proportion of DHA (41%) compared to the bovine retina (26%) (Fig. 2e), and that VLC-PUFAs constituted 45% of total retinal lipids in the Greenland shark, compared to 35% in mammals. Moreover, the dominant VLC-PUFAs of the Greenland shark featured longer carbon chains (36 carbons) compared to the bovine ones (32 carbons; Fig. 2e) or to mouse[72]. The higher proportion of PUFAs and the longer carbon chains in the Greenland shark compared to other vertebrates might represent yet another adaptation to the deep-sea environment, as recently proposed[73]. Taken together, our data show that the lipid composition of disc membranes in Greenland shark appears to be optimal to support rhodopsin function.

Rhodopsin spectral sensitivity and corneal light transmission in the Greenland shark

In vertebrates, the spectral sensitivity of the visual pigment formed by the rod opsin is typically tuned to the prevailing wavelengths of light in the environment[22]. This is also true for the Greenland shark. Spectroscopic analysis of purified, in vitro-expressed Greenland shark rhodopsin bound to 11-*cis*-retinal revealed a maximum absorbance wavelength (λ_{max}) of 458 nm (Fig. 3b), which is shorter than that of most shallow-dwelling sharks[58], and even particularly blue-shifted compared to other deep-sea species[49]. Short-wavelength shifting of the rhodopsin λ_{max} is a typical adaptation found in deep-sea fishes[49], suggesting adaptive evolution of the Greenland shark rhodopsin for life in the deep sea. Furthermore, the extreme blue-shift observed in the Greenland shark rhodopsin may reflect adaptation to the highly transparent, blue-dominated light environments of deep, high-latitude Arctic waters[74].

Finally, we investigated whether the parasitized cornea of the Greenland shark allows penetration of light to the retina. Using a SpectralLED tunable light source coupled to an integrating sphere and a spectroradiometer (Fig. 3c), we measured light transmission through fixed Greenland shark corneas compared to fixed human donor corneas (Fig. 3d). All shark corneas analysed had parasites bound to the corneal edges (Fig. S47). We found that human corneas had an average transmittance of 95%, while the six shark corneas ranged from 70 to 100% transmittance. In the blue light range specifically (450–500 nm), human corneas had an average transmittance of 94%, while the shark corneas ranged from 66 to 100% transmittance. These findings suggest that Greenland shark corneas allow light to reach the retina, despite the presence of parasites.

Retinal gene expression in the Greenland shark

Given that we found a fully intact phototransduction gene repertoire and cell circuitry for rod-based vision in the Greenland shark, we sought to determine whether the expression levels of the phototransduction genes were comparable to those in other shark species and thus, biologically relevant. To address this, we sequenced bulk retinal transcriptomes from the Greenland shark and compared them to publicly available transcriptomic data from retinas of five representative shark species: *S. canicula, S. torazame, I. oxyrinchus, R. typus*, and *C. plagiosum*. Our analysis revealed that key rod phototransduction genes were expressed at biologically relevant levels in the retina of the Greenland shark, including rhodopsin (*rh1*), rhodopsin kinase (*grk1*), arrestin (*sag*), transducins (*gnat1* and *gngt1*), and phosphodiesterases (*pde6a, pde6b*, and *pde6g*) (Fig. 4b). Expression levels of these genes were found to be comparable to those observed in adult specimens of other shark species (*S. canicula*, *S. torazame*, and *C. plagiosum*) and higher than those in species sampled as juveniles (*I. oxyrinchus* and *R. typus*) (Fig. 4b). In contrast, we observed either no expression or low expression of cone phototransduction genes in the Greenland shark (Fig. 4c), consistent with a visual system specialized for scotopic vision. Interestingly, individuals from our comparison group that were juveniles (*e.g., I. oxyrinchus* and *R. typus*) exhibited relatively lower levels of most phototransduction genes compared to adults from other species. While these patterns may reflect developmental differences, we acknowledge that species and life stage are not fully independent in our dataset, and this may contribute to the observed variation. Overall, our findings suggest that the Greenland shark preferentially relies on rod-based phototransduction for vision. The transcriptomic basis for scotopic vision in this species is fully intact, comparable to other adult elasmobranchs, and well-suited to its dim light environment.

Lastly, we investigated whether efficient DNA repair mechanisms may contribute to the preservation of retinal structure and maintenance of photoreceptor integrity in the retina of the Greenland shark, as has been suggested for other organisms and recently shown in the bowhead whale[75]. Specifically, we focused on the ERCC1-XPF DNA repair complex which is known to have an important role in supporting retinal health and has been linked to retinal aging across a range of eukaryotes[40,76–81]. Notably, UV sensitivity and early-onset vision loss are hallmarks of the human progeroid syndrome, Xeroderma Pigmentosum, caused by mutations in the ERCC1-XPF complex[82]. Similarly, *ercc1* knockout mice exhibit accelerated retinal aging and degeneration[40], highlighting the complex's role in protecting ocular tissues. We found that shark species with the longest lifespans, including the Greenland shark, retain the *ercc1* gene, while shorter-lived sharks lacked this gene[83–88], and that the Greenland shark exhibits elevated expression of *ercc4 (xpf)* compared to other sharks (Fig. 3d). This suggests that a robust DNA repair system may help preserve retinal integrity and function over the extremely long lifespan of the Greenland shark. Future studies could help clarify the role of the ERCC1–XPF complex in retinal maintenance in sharks and may reveal

https://doi.org/10.1038/s41467-025-67429-6

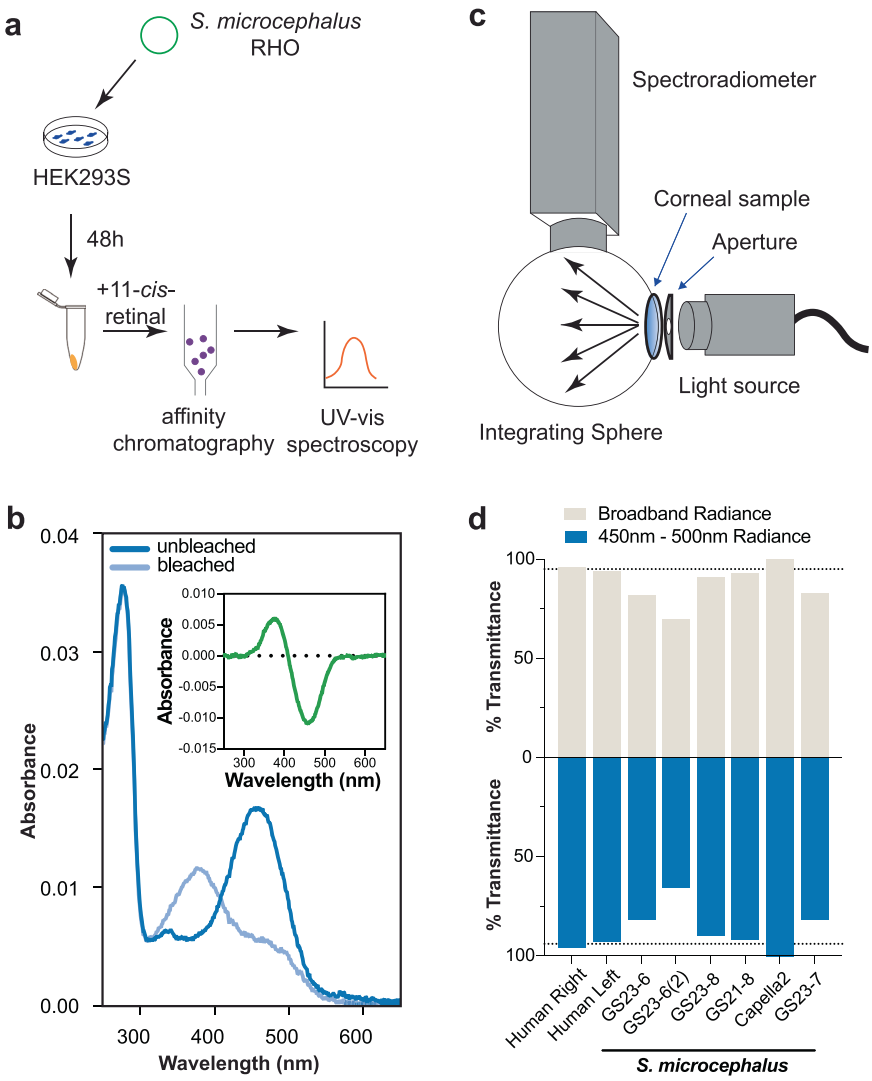

Fig. 3 | Visual pigment spectral sensitivity and corneal transmission in the Greenland shark. a Workflow for expression and immunoaffinity purification of *S. microcephalus* rhodopsin reconstituted with 11-*cis*-retinal in HEK293S cells, followed by UV-vis spectroscopy analysis. **b** UV-vis spectroscopic measurements of *S. microcephalus* rhodopsin. Inset depicts the difference (between bleached and unbleached) spectra. **c** Schematic optical setup used for measuring corneal transmittance. **d** Corneal transmittance of human and *S. microcephalus* samples. *Top:* broadband radiance measurements (425–600 nm); *bottom:* focused blue light range (450–500 nm). Dashed lines indicate the average percentage (%) transmittance between right and left human corneas. Source data are provided as a Source Data file.

additional DNA repair pathways that contribute to visual longevity in this species.

Preservation of vision over centuries

Our findings provide compelling evidence that the Greenland shark (*S. microcephalus*) retains functional vision, despite extreme longevity, corneal parasitisation, and an environment characterized by minimal light. The rod phototransduction pathway remains intact, and the loss or pseudogenization of most cone pathway genes strongly suggests a reliance on scotopic vision. Active transcription of rod phototransduction pathway genes, supported by RNA-seq, RNAscope and chromatin staining, indicates that the retina is functionally preserved. Furthermore, key visual adaptations revealed by histological analyses and in vitro opsin expression are well-aligned with the deep-sea ecology of this species, including elongated, densely packed rods and a short-wavelength shift in rhodopsin sensitivity. In addition, corneal transmission remains intact despite chronic parasitism. The absence of obvious retinal degeneration in exceptionally old individuals, alongside the preferential retention and elevated expression of DNA repair genes linked to retinal degeneration (*ercc1*, *ercc4*), suggests a potential mechanism underpinning their long retinal health span. Together, these findings highlight the extraordinary adaptability of vertebrate sensory systems in extreme environments and the remarkable preservation of organ function over hundreds of years.

Methods

Animal tissue collection and preservation

The Greenland sharks used in this study were caught between 2020 and 2024 using scientific long lines off the coast of the University of Copenhagen's Arctic Station on Disko Island, Greenland (69°15′N, 53°34′W). All sampling was carried out in accordance with laws and regulations under a permit to collect Greenland sharks for scientific purposes. The work was carried out with authorisation from the Government of Greenland under permits (2020-26794, 2022-24744, 2023-6108, 2024-119) from the Ministry of Fisheries, Hunting & Agriculture and a non-exclusive licence (G24-051) for the utilization of Greenland genetic resources issued by the Ministry of Foreign Affairs, Business

https://doi.org/10.1038/s41467-025-67429-6

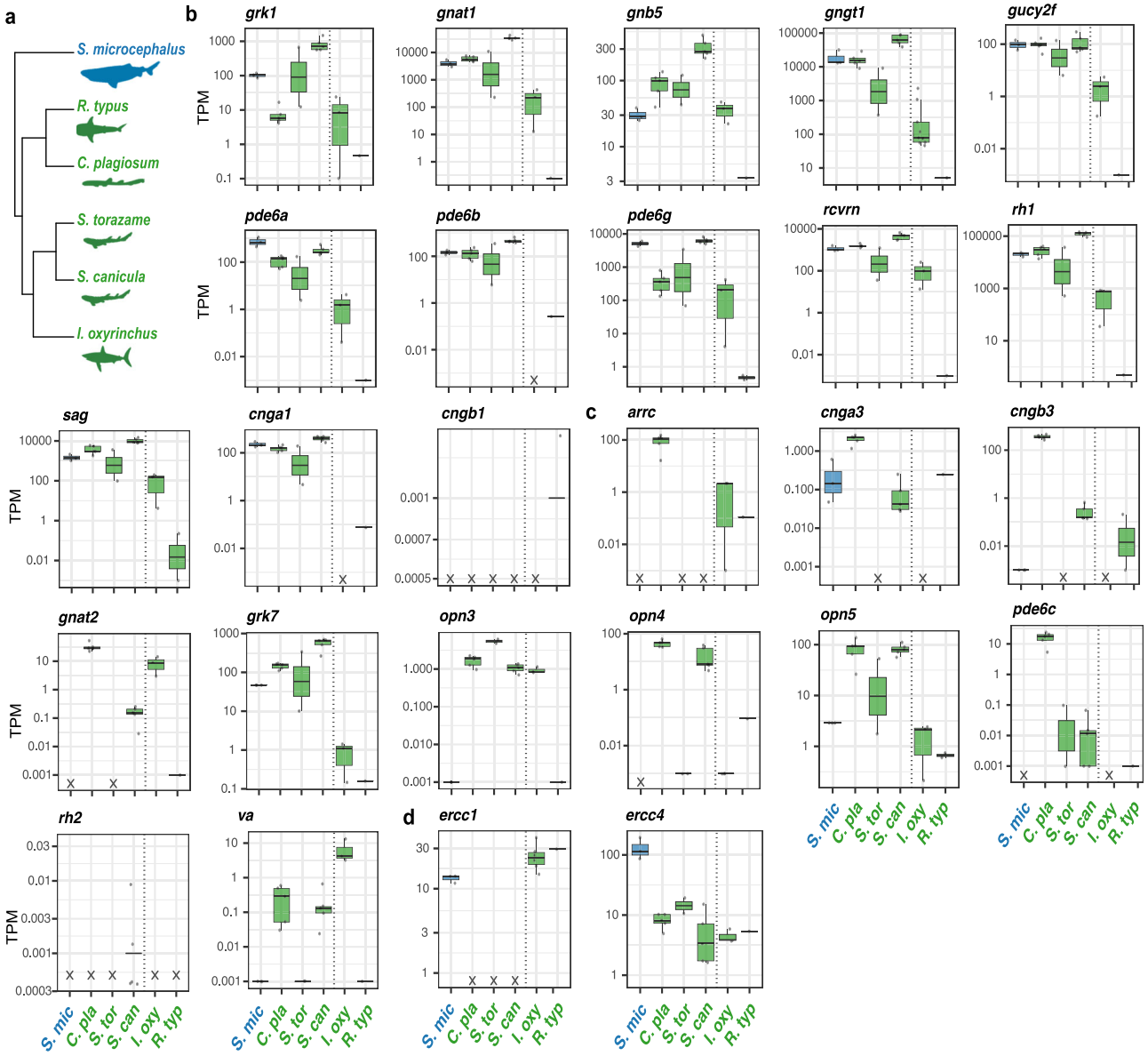

Fig. 4 | Transcriptomic basis of vision in the Greenland shark. a Phylogeny of species used for gene expression analyses. **b**–**d** Retinal expression of genes involved in rod-based phototransduction (**b**), cone-based or non-visual photoreception (**c**) and DNA repair (**d**) in *Somniosus microcephalus* (blue; $n = 3$ individuals) and five comparison species (green; *Scyliorhinus canicula* [$n = 5$], *S. torazame* [$n = 2$], *Isurus oxyrinchus* [$n = 3$], *Rhincodon typus* [$n = 1$], and *Chiloscyllium plagiosum* [$n = 5$]). Species names have been abbreviated. Data are transcripts per million (TPM) plotted on a log-scaled axis. Data are presented as box plots (centre line at the median, upper bound at 75th percentile, lower bound at 25th percentile) with whiskers at minimum and maximum values. Dotted line demarcates data derived from transcriptomes from adult (left) and juvenile (right) specimens. Genes which were not retrieved or were pseudogenized are marked with a cross. Note that some genes given in (**b**) are involved in all types of phototransduction (*i.e., rvcrn, grk1, gnb5* and *gucy2f*). Source data are provided as a Source Data file.

and Trade. Individuals were euthanized immediately after capture by direct spinal cord transection. Total body length (TL) was measured, and eyecups were dissected and either fixed whole in 4% paraformaldehyde [PFA; 4% (w/v) PFA in 0.01 M phosphate-buffered saline] or the retina was removed and fixed in RNAlater or 100% ethanol. Ages were estimated from TL based on the values provided in Nielsen et al. (2016), which were calculated using the von Bertalanffy growth model[2]. Details of all individuals can be found in Table S1.

The bovine eyes used in this study ($n = 5$) were obtained from a commercial slaughterhouse. Each eye was dissected to remove the anterior segment, lens, and vitreous. The retina was then carefully separated from the underlying eyecup and stored at −80 °C until further processing.

Human donor tissue collection and preservation

The human donor eyes used in this study were obtained and managed in compliance with the Declaration of Helsinki. De-identified eyeballs from a 50-year-old female donor were obtained from the Willed Body Program at the University of California, Irvine (Irvine, CA) within 12 h postmortem, in compliance with ethical requirements of the program. The program is registered with the respective state boards to facilitate the distribution of deceased human remains for research purposes. Prior to tissue processing, serological testing was performed on donor blood to exclude samples positive for blood-borne pathogens. Whole eyes were dissected, the anterior segments were further isolated and 5 mm bio punches were taken for further analysis. All samples are preserved in the laboratory of Dorota Skowronska-Krawczyk.

Retinal histology

Retinal morphology was assessed for one PFA-fixed eye each from three adult specimens of *S. microcephalus*. Whole, enucleated eyes were post-fixed in 2.5% glutaraldehyde and 2% PFA in 0.1 M PBS, progressively dehydrated in increasing concentrations of ethanol, infiltrated with EMbed-812 resin and polymerized at 60 ° C for 48 h. For light micrographs, 1 µm-thick radial sections were cut on a Reichert-Jung Ultracut E ultramicrotome, deplastified, stained with epoxy tissue stain (Electron Microscopy Sciences; toluidine blue and basic fuchsin), and imaged under brightfield illumination on a Leica DM4 microscope.

Additionally, hematoxylin and eosin (H&E) staining was performed on 4 µm-thick paraffin sections from a separate eye. Sections were processed following a standard protocol[89]: deparaffinized in xylene, rehydrated through a graded ethanol series to distilled water, stained with hematoxylin for 5 min, rinsed in running tap water, differentiated in 1% acid alcohol, and blued in an alkaline solution. Counterstaining with eosin was carried out for 1–2 min, followed by dehydration through graded ethanol, clearing in xylene, and mounting.

Whole-genome sequencing

A draft genome was sequenced for the Greenland shark, *S. microcephalus*. Briefly, DNA was extracted from frozen tissue from two adult retinas using Zymo Quick-DNA Miniprep Plus kit. DNA quality was assessed on an Agilent TapeStation and library preparation and sequencing was performed by the Department of Biosystems Science and Engineering (ETH Zurich). Individual libraries were prepared using NEBNext Ultra II FS DNA Library Prep kit (Illumina) with 150 bp insert size, pooled, and sequenced as 150 bp paired-end reads on an Illumina NovaSeq6000 with an SP flow cell (300 cycles). Quality control and adapter removal were performed with fastp (v.0.23.4)[90], filtered reads were assembled using ABySS (v.2.3.1) using a k-mer size of 80 and k-mer coverage threshold of two[91] and the completeness of the assembly was assessed using BUSCO (v.5.4.5) using the vertebrata odb10 database[92] (see Table S3 for assembly statistics).

Chondrichthyes phylogeny

A species tree was constructed for 17 species in the class Chondrichthyes (see Table S2 for accession numbers). All genome assemblies available for Chondrichthyes were downloaded from the NCBI Genome database. Completeness of each genome was assessed using BUSCO (v.5.4.5) using the vertebrata odb10 database and assemblies with completeness scores over 80% were retained (14 species). An additional three species were included in the phylogeny: *S. microcephalus* and another two species which were used for phototransduction gene mining and expression analyses (*S. torazame*, 76.0% complete; *R. typus*, 75.6% complete). All single-copy orthologs (obtained from BUSCO analysis) present in at least half of the species were aligned using MUSCLE (v.5.1)[93], alignments were trimmed using trimAl (v.1.4.1)[94], and maximum likelihood trees were made for each ortholog using IQ-TREE (v.2.0)[95]. An unrooted species tree was estimated by inputting concatenated gene trees into ASTRAL (v.5.7.8)[96], and the tree was dated and rooted using the least-squared method in IQ-TREE and visualised in iTOL (v.6.9.1)[97].

Phototransduction and DNA repair gene mining

Phototransduction and DNA repair genes were mined from the newly generated draft genome assembly for *S. microcephalus* and from published genome assemblies for five other shark species (*S. canicula*, GCF_902713615.1_sScyCan1.1[98]; *S. torazame*, GCA_003427355.1_Storazame_v1.0[99], *R. typus*, GCF_021869965.1_sRhiTyp1.1[100]; *I. oxyrinchus*, GCA_026770705.1[101]; and *C. plagiosum*, GCF_004010195.1[102]), which were selected because they also had publicly available RNAseq data. Genome annotations were obtained for all NCBI genomes, except for *I. oxyrinchus*. The *I. oxyrinchus* genome assembly was annotated by inputting publicly available RNAseq data for this species (see Table S2 for NCBI accession numbers), protein annotations for the four other shark species, and Vertebrata orthologs from OrthoDB (v.12.0)[103] into BRAKER (v.3)[104].

For *S. microcephalus*, phototransduction and DNA repair gene coding sequences (CDS) were mined using a combination of exon prediction and mapping guided by publicly available reference sequences from NCBI. For the opsin genes, we specifically searched for all known genes (including *rh1, sws1, sws2, lws*, and *rh2*) using multiple reference species. For the exon prediction approach, scaffolds of interest in the genome assembly were identified using TBLASTN (v.2.11.0)[105] and EXONERATE (v.2.4.0)[106] was used to predict exons on those scaffolds similar to reference sequences. If the exon prediction approach did not yield a CDS, or if the CDS was fragmented, the CDS was retrieved or completed using a mapping approach. Briefly, raw genomic reads were mapped to reference sequences using HISAT2 (v.2.2.1)[107] and the consensus sequence was extracted in Geneious Prime (v.2022.2.2; Biomatters Ltd).

Phototransduction and DNA repair genes were also mined from another five shark species with publicly available genome assemblies. For *S. canicula, R. typus* and *C. plagiosum*, functional genome annotations were available and thus, genes were mined by filtering the annotation (GFF) file to keep only matched gene names and AGAT (v.1.4.1)[108] was used to extract the CDS for the longest isoform per gene. For the two species without functional genome annotations (*S. torazame* and *I. oxyrinchus*), all genes were mined using the exon prediction approach described above and annotation files were manually edited to incorporate mined genes.

The identity of every gene mined was confirmed phylogenetically. To that end, gene trees for each clade of interest were generated by downloading reference sequences for outgroup species (*Homo sapiens, Mus musculus* and *Danio rerio*) and other chondrichthyan species from NCBI, aligning these with mined genes using MUSCLE, trimming alignments using trimAl, generating maximum likelihood phylogenies using IQ-TREE and rooting in iTOL (Fig. S2-S12).

Selection tests on phototransduction and DNA repair genes

The selective forces acting on the newly mined genes were assessed for *S. microcephalus*. For each gene clade, the protein sequences of the Greenland shark were aligned with those from other species in Chondrichthyes using MUSCLE (after removing stop codons and frameshifts present in pseudogene sequences). This protein alignment was then converted to a codon alignment using trimAl and used to construct a gene tree for each clade using IQ-TREE. The codon alignment and the corresponding gene tree were then used to compute maximum likelihood estimates of ω with PAML. Three branch models were used: (i) a free-ratio model, which allows a different ω value per branch; (ii) a two-ratio model assuming one ω for the Greenland shark branches and one ω for all other branches; and (iii) a null one-ratio model assuming that every branch has the same ω ratio. For all genes, the best model was always the free-ratio model (Model 1). The choice between Model 2 and Model 3 was always made using the mean of a likelihood ratio test, using the $\chi 2$ distribution with one degree of freedom. Finally, for each gene clade, RELAX[109] and aBSREL[110] was implemented via the HyPhy framework (v.2.5.63)[111] to look for signs of relaxed selection or positive selection in the Greenland shark genes. Greenland shark branches were assigned as "test" branches, while all other branches were assigned as background branches, in sequential runs of RELAX and aBSREL.

Rhodopsin absorption spectrum measurements

The peak spectral sensitivity of the *S. microcephalus* rhodopsin (RHO) was assessed using in vitro protein regeneration and spectrophotometry (Fig. 3a). In brief, HEK293S cells were transfected to

express Greenland shark RHO modified to contain the 1D4 epitope derived from the C-terminus of bovine rhodopsin (TETSQVAPA). The plasmid, pRP[Exp]-CBA-[SharkRH1], was constructed and packaged by VectorBuilder (vector ID: VB241011-1418sns). After 48 h, cells were pelleted down for 1D4-affinity chromatography. Immunoaffinity 1D4 resin was prepared by conjugating purified, anti-Rho antibody (1D4) to CNBr-activated Sepharose 4B beads (Cytiva). Pelleted cells were homogenized, and RHO pigments were reconstituted with 40 μM 11-*cis*-retinal for 1 h at room temperature to regenerate RHO from apo-opsin. Then, 10% DDM was added to solubilize the membrane-enriched pellet, followed by 1 h incubation at 4 °C and centrifugation (21,300 x g) for 5 min at 4 °C. The supernatant was then filtered through a 0.22 μm polyethersulfone membrane and incubated with 250 μL of 1D4-resin for 1 h at 4 °C. Rho-1D4-resin mixture was loaded onto a centrifuge column, washed in a buffer containing 50 mM HEPES (pH 7.5), 0.25 M NaCl, and 10% DDM, and eluted with C-terminal non-apeptide (synthesized by GenScript, NJ, USA) overnight at 4 °C. Absorption spectra were recorded using a Varian Cary 50 Scan UV-Vis spectrophotometer (Varian Australia Pty Ltd). The unbleached sample was used as blank, after which the sample was bleached for 10 min with a white-light, 875-Lumens bulb. The difference in absorption spectrum was then recorded.

Nuclear chromatin staining and quantification

Eyecups were fixed in 4% PFA overnight, cryoprotected by immersion in a sucrose gradient (10% and 20% sucrose for 1 h at room temperature, and 30% sucrose overnight at 4 °C), embedded in Tissue-Tek OCT (Sakura, Torrance, CA) and frozen on a conductive metal block placed on dry ice. After cryosectioning, sections were blocked in 5% bovine serum albumin (BSA), 0.3% TritonX-100 for 1.5 h at room temperature to minimize nonspecific binding. Sections were then incubated with primary antibodies (mouse anti-trimethyl histone H4 (sc-134216), 1:200 and rabbit anti-H3K27ac (ab-4729), 1:200) diluted in 5% BSA and 0.1% TritonX-100 overnight at 4 °C. Following three washes with PBS, sections were incubated with fluorescently-labeled secondary antibodies diluted in 5% BSA and 0.1% TritonX-100 for 1 h at room temperature. Following three washes with PBS, nuclei were counterstained with Hoescht 33342 (Thermo), and sections were mounted using ProLong Gold Antifade (Thermo). Immunostained sections were imaged on a Zeiss LSM900 confocal microscope with Airyscan 2 at 40X magnification. Quantification of nuclear chromatin distribution was performed using ImageJ. For each cell, two straight lines were drawn across the nucleus, and intensity profiles for the H4K20me3, H3K27ac, and Hoechst channels were measured. The intensity profiles were normalized within each channel and plotted against the normalized distance along each line.

Fluorescence in situ hybridization

In situ hybridization was performed using the RNAscope® Multiplex Fluorescent Assay v2 (ACD Diagnostics) following modifications[112]. Briefly, frozen histologic sections of fixed shark eyes were pre-treated as per the manual using hydrogen peroxide and target retrieval reagents, including protease IV. Probes were then hybridized according to the protocol and then detected with TSA Plus® Fluorophores fluorescein, cyanine 3, and cyanine 5. Sections were mounted with Prolong Gold Antifade (Thermo Fisher) and imaged (Keyence BZ-X700). Probes specific for mouse and human transcripts were designed by the manufacturer (see Table S5).

TUNEL assay

DNA fragmentation was detected using the Click-iT™ Plus TUNEL Assay Kit, Alexa Fluor™ 488 (Thermo Fisher Scientific, C10617), following the manufacturer's protocol. As a positive control for DNA fragmentation, selected sections were treated with 1U DNase I for 30 min at 37 °C. Slides were counterstained with Hoechst 33342 and images were acquired using a Zeiss LSM900 confocal microscope with Airyscan 2 at 20X magnification.

Fatty acid analysis

Lipid purification and fatty acid quantification were performed following the method of Gao and colleagues[113]. Briefly, lipids from *B. taurus* ($n = 5$) and *S. microcephalus* ($n = 2$) retinas were extracted according to the methodology of Bligh and Dyer[114]. Specifically, the tissue was homogenized in 200 μL water, transferred to a glass vial, and 750 μL 1:2 (v/v) $CHCl_3$: MeOH was added and vortexed. Then, 250 μL $CHCl_3$ was added and vortexed. Finally, 250 μL ddH_2O was added and vortexed. The samples were centrifuged at 3000 RPM for 5 min at 4 °C. The lower phase was transferred to a new glass vial and dried under nitrogen stored at -20 °C until subsequent lipid analysis. The total fatty acids were released through acid hydrolysis and extracted with hexane, then the sample was evaporated under nitrogen and stored at -20 °C until subsequent lipid analysis. LC-MS/MS separation of VLC-PUFAs was achieved on an Acquity UPLC® BEH C18 column (1.7 μm, 2.1 × 100 mm, Waters Corporation). The Q Exactive mass spectrometer (Thermo Fisher Scientific) was operated in a full MS scan mode (resolution 70,000 at m/z 200) in negative mode. For the compounds of interest, a scan range of m/z 250–800 was chosen. The identification of fatty acids was based on retention time and formula.

Corneal transmittance

We measured light transmission through 5 mm diameter bio-punches of six corneas from five Greenland sharks and a pair of corneas from a human donor for reference. Using a SpectralLED tunable light source coupled to an integrating sphere and a spectroradiometer (PhotoResearch-655 SpectraScan®), we measured spectral radiance of samples between wavelengths 425–600 nm as shown in the optical setup in Fig. 3c. Transmittance was calculated as a % representing the ratio between the radiance measurements of corneal samples to reference radiance (no corneas).

Retinal transcriptome sequencing

Retinal transcriptomes were sequenced for three individuals for *S. microcephalus*. Briefly, total RNA was extracted from one RNAlater-fixed retina from each of three adult sharks using the QuickRNA Miniprep kit (Zymo). RNA quality was assessed on an Agilent TapeStation and library preparation and sequencing was performed by the Department of Biosystems Science and Engineering (ETH Zurich). Individual libraries were prepared using TruSeq stranded total RNA ribo-zero gold kit (Illumina), pooled, and sequenced as 100 bp paired-end reads using BRAVO Sequencing on an Illumina NovaSeq6000 with an S4 flow cell (200 cycles). Quality control and adapter removal was performed with fastp (v.0.23.4).

Phototransduction and DNA repair gene expression

Phototransduction and DNA repair gene expression was quantified for the Greenland shark and five other shark species for which retinal transcriptome data were available on NCBI (see Table S2 for accession numbers). For the five other species, transcriptomes were pre-processed using fastp and mapped to annotated genomes using STAR (v.2.7.10b)[115] with --outFilterMultimapNmax 1 --outFilterMatchNminOverLread 0.4 --outFilterScoreMinOverLread 0.4 options, and mapped singletons were filtered out for paired-end data. Read counts were performed using the HTSeq-count script from the HTSeq framework (v.2.0.2)[116] and were used to calculate TPM values for all genes. For the genes of interest, TPM values were plotted against the proportion of reads mapped (calculated as the number of reads mapped divided by the total number of reads in the transcriptome) in R (v.4.4.0)[117] and a linear regression was performed to generate an equation that describes the relationship between the two variables for each gene (Fig. S44).

For the Greenland shark, an annotation file was manually generated for all genes that were mined, and this was used to guide mapping against those sequences using STAR. Similar to the other species, mapped singletons were filtered out and read counts were performed using HTSeq-count. The equations generated using the other five shark species were used to extrapolate TPM values from the proportion of mapped reads for each gene expressed in the Greenland shark.

Reporting summary

Further information on research design is available in the Nature Portfolio Reporting Summary linked to this article.

Data availability

Newly identified coding sequences (PV442159-PV442194; https://www.ncbi.nlm.nih.gov/nuccore/?term=PV442159:PV442194[accn]) as well as raw genomic and transcriptomic reads and genome assembly are available through GenBank (PRJNA1246101; https://www.ncbi.nlm.nih.gov/bioproject/PRJNA1246101) and the NCBI Sequencing Read Archive (see Table S2 for accession numbers). All other data are available via Figshare (https://figshare.com/s/9d86a7c9eccced4c6505) or are provided in the main manuscript or Supplementary Information. Source data are provided with this paper.

References

1. Bloch, M.E. and J.G. Schneider. *M.E. Blochii*, Systema ichthyologiae iconibus CX illustratum. Vol. [Atlas]. Berolini: Sumtibus auctoris impressum et Bibliopolio Sanderiano commissum. (Bavarian State Library, 1801).
2. Nielsen, J. et al. Eye lens radiocarbon reveals centuries of longevity in the Greenland shark (Somniosus microcephalus). *Science* **353**, 702 (2016).
3. Nielsen, J., Hedeholm, R. B., Simon, M. & Steffensen, J. F. Distribution and feeding ecology of the Greenland shark (Somniosus microcephalus) in Greenland waters. *Polar Biol.* **37**, 37–46 (2014).
4. Mecklenburg, C. et al. Marine Fishes of the Arctic Region. Conservation of Arctic Flora and Fauna. Vol. 1. Akureyri, Iceland. (2018).
5. MacNeil, M. A. et al. Biology of the Greenland shark Somniosus microcephalus. *J. Fish. Biol.* **80**, 991–1018 (2012).
6. Berland, B. Copepod Ommatokoita elongata (Grant) in the eyes of the Greenland Shark—a possible cause of mutual dependence. *Nature* **191**, 829–830 (1961).
7. Kabata, Z. *Parasitic Copepoda of British Fishes*. (Ray Society, 1979).
8. Borucinska, J. D., Benz, G. W. & Whiteley, H. E. Ocular lesions associated with attachment of the parasitic copepod Ommatokoita elongata (Grant) to corneas of Greenland sharks, Somniosus microcephalus (Bloch & Schneider). *J. Fish. Dis.* **21**, 415–422 (1998).
9. Skomal, G. B. & Benz, G. W. Ultrasonic tracking of Greenland sharks, Somniosus microcephalus, under Arctic ice. *Mar. Biol.* **145**, 489–498 (2004).
10. Nielsen, J. et al. Greenland Shark (Somniosus microcephalus) stomach contents and stable isotope values reveal an ontogenetic dietary shift. *Front. Mar. Sci.* **6**, 125 (2019).
11. Lamb, T. D. Why rods and cones? *Eye* **30**, 179–85 (2016).
12. Lamb, T. D. Evolution of phototransduction, vertebrate photoreceptors and retina. *Prog. Retin. Eye Res.* **36**, 52–119 (2013).
13. de Busserolles, F., Fogg, L., Cortesi, F. & Marshall, J. The exceptional diversity of visual adaptations in deep-sea teleost fishes. *Semin. Cell Dev. Biol.* **106**, 20–30 (2020).
14. Fogg, L. G. et al. Development of dim-light vision in the nocturnal reef fish family Holocentridae I: retinal gene expression. *J. Exp. Biol.* **225**, jeb244513 (2022).
15. Fogg, L. G. et al. Development of dim-light vision in the nocturnal reef fish family Holocentridae II: retinal morphology. *J. Exp. Biol.* **225**, jeb244740 (2022).
16. Fogg, L. G. et al. Deep-sea fish reveal alternative pathway for vertebrate visual development. bioRxiv: 2024.10.10.617579. https://doi.org/10.1101/2024.10.10.617579 (2024).
17. Cortesi, F. et al. Visual system diversity in coral reef fishes. *Semin. Cell Develop. Biol.* **106**, 31–42 (2020).
18. Lythgoe, J. N. *The Ecology of Vision*. (Clarendon Press, 1979).
19. Munz, F.W. and W.N. McFarland, Evolutionary Adaptations of Fishes to the Photic Environment, in *The Visual System in Vertebrates*. (Springer-Verlag, 1977).
20. Carleton, K. L., Dalton, B. E., Escobar-Camacho, D. & Nandamuri, S. P. Proximate and ultimate causes of variable visual sensitivities: Insights from cichlid fish radiations. *Genesis* **54**, 299–325 (2016).
21. Carleton, K. L., Escobar-Camacho, D., Stieb, S. M., Cortesi, F. & Marshall, N. J. Seeing the rainbow: mechanisms underlying spectral sensitivity in teleost fishes. *J. Exp. Biol.* **223**, jeb193334 (2020).
22. Musilova, Z., Salzburger, W. & Cortesi, F. The visual opsin gene repertoires of teleost fishes: evolution, ecology, and function. *Annu. Rev. Cell Develop. Biol.* **37**, 441–468 (2021).
23. Hauzman, E. Adaptations and evolutionary trajectories of the snake rod and cone photoreceptors. *Semin. Cell Develop. Biol.* **106**, 86–93 (2020).
24. de Busserolles, F. & Marshall, N. J. Seeing in the deep-sea: visual adaptations in lanternfishes. *Philos Trans R Soc Lond B Biol Sci.* **372**, https://doi.org/10.1098/rstb.2016.0070 (2017).
25. Delroisse, J., Duchatelet, L., Flammang, P. & Mallefet, J. De novo transcriptome analyses provide insights into opsin-based photoreception in the lanternshark Etmopterus spinax. *PLoS One* **13**, e0209767 (2018).
26. Claes, J. M. et al. Photon hunting in the twilight zone: visual features of mesopelagic bioluminescent sharks. *PloS one* **9**, e104213 (2014).
27. Denton, E. J. & Shaw, T. I. The visual pigments of some deep-sea elasmobranchs. *J. Mar. Biol. Assoc. U.K.* **43**, 65–70 (1963).
28. Newman, A. S., Marshall, J. N. & Collin, S. P. Visual eyes: a quantitative analysis of the photoreceptor layer in deep-sea sharks. *Brain Behav. Evol.* **82**, 237–249 (2013).
29. Hart, N. S. Vision in sharks and rays: opsin diversity and colour vision. *Semin. Cell Develop. Biol.* **106**, 12–19 (2020).
30. Policarpo, M. et al. Contrasting gene decay in subterranean vertebrates: insights from cavefishes and fossorial mammals. *Mol. Biol. Evol.* **38**, 589–605 (2020).
31. Simon, N., Fujita, S., Porter, M. & Yoshizawa, M. Expression of extraocular opsin genes and light-dependent basal activity of blind cavefish. *PeerJ* **7**, e8148 (2019).
32. Protas, M. & Jeffery, W. R. Evolution and development in cave animals: from fish to crustaceans. *WIREs Develop. Biol.* **1**, 823–845 (2012).
33. Stokesbury, M., Harvey-Clark, C., Hay Gallant, J., Block, B. & Myers, R. Movement and environmental preferences of Greenland sharks (Somniosus microcephalus) electronically tagged in the St. Lawrence Estuary, Canada. *Mar. Biol.* **148**, 159–165 (2005).
34. Edwards, J. E. et al. Advancing research for the management of long-lived species: a case study on the greenland shark. *Front. Mar. Sci.* **6**, 87 (2019).
35. Yopak, K. E. et al. Comparative brain morphology of the greenland and pacific sleeper sharks and its functional implications. *Sci. Rep.* **9**, 10022 (2019).
36. Bartas, M. et al. RNA analysis of the longest living vertebrate Greenland shark revealed an abundance of LINE-like elements in its transcriptome. *Czech Polar Rep.* **13**, 17 (2024).
37. Peel, L. R., Collin, S. P. & Hart, N. S. Retinal topography and spectral sensitivity of the Port Jackson shark (Heterodontus portusjacksoni). *J. Comp. Neurol.* **528**, 2831–2847 (2020).

38. Schieber, N. L., Collin, S. P. & Hart, N. S. Comparative retinal anatomy in four species of elasmobranch. *J. Morphol.* **273**, 423–440 (2012).
39. Kumar, P. et al. Experimental oral iron administration: histological investigations and expressions of iron handling proteins in rat retina with aging. *Toxicology* **392**, 22–31 (2017).
40. Narasimhan, A. et al. The Ercc1(-/Δ) mouse model of XFE progeroid syndrome undergoes accelerated retinal degeneration. *Aging Cell* **15**, e14419 (2024).
41. Nag, T. C., Maurya, M. & Roy, T. S. Age-related changes of the human retinal vessels: possible involvement of lipid peroxidation. *Ann. Anat.* **226**, 35–47 (2019).
42. Cho, N. C., Poulsen, G. L., Ver Hoeve, J. N. & Nork, T. M. Selective loss of S-cones in diabetic retinopathy. *Arch. Ophthalmol.* **118**, 1393–400 (2000).
43. Gao, H. & Hollyfield, J. G. Aging of the human retina. Differential loss of neurons and retinal pigment epithelial cells. *Invest Ophthalmol. Vis. Sci.* **33**, 1–17 (1992).
44. Curcio, C. A., Millican, C. L., Allen, K. A. & Kalina, R. E. Aging of the human photoreceptor mosaic: evidence for selective vulnerability of rods in central retina. *Invest Ophthalmol. Vis. Sci.* **34**, 3278–96 (1993).
45. Curcio, C. A. & Drucker, D. N. Retinal ganglion cells in Alzheimer's disease and aging. *Ann. Neurol.* **33**, 248–257 (1993).
46. Freed, J. et al. The elephant retina examined across a range of ages. bioRxiv: 2021.01.20.427452. https://doi.org/10.1101/2021.01.20.427452 (2021).
47. da Silva, R., Conde, D. A., Baudisch, A. & Colchero, F. Slow and negligible senescence among testudines challenges evolutionary theories of senescence. *Science* **376**, 1466–1470 (2022).
48. Do, M. T. H. Melanopsin and the intrinsically photosensitive retinal ganglion cells: biophysics to behavior. *Neuron* **104**, 205–226 (2019).
49. Musilova, Z. et al. Vision using multiple distinct rod opsins in deep-sea fishes. *Science* **364**, 588–592 (2019).
50. Lupše, N. et al. Visual gene expression reveals a cone-to-rod developmental progression in deep-sea fishes. *Mol. Biol. Evol.* **38**, 5664–5677 (2021).
51. Bacchet, P., T. Zysman and Y. Lefevre. *Guide des poissons de Tahiti et ses iles*. 4th ed. (Tahiti, 2016).
52. Weigmann, S. Annotated checklist of the living sharks, batoids and chimaeras (Chondrichthyes) of the world, with a focus on biogeographical diversity. *J. Fish. Biol.* **88**, 837–1037 (2016).
53. Bianchi, G. et al. *Field Guide to the Living Marine Resources of Namibia*. FAO species identification guide for fishery purposes. (FAO, 1999).
54. Capapé, C. et al. Maturity, fecundity and occurrence of the smallspotted catshark Scyliorhinus canicula (Chondrichthyes: Scyliorhinidae) off the Languedocian coast (southern France, north-western Mediterranean). *Vie et Milieu/Life & Environ.* **58**, 47–55 (2008).
55. Ito, N., Fujii, M., Nohara, K. & Tanaka, S. Scyliorhinus hachijoensis, a new species of catshark from the Izu Islands, Japan (Carcharhiniformes: Scyliorhinidae). *Zootaxa* **5092**, 331–349 (2022).
56. Hart, N. S. et al. Widespread and convergent evolution of cone monochromacy in galeomorph sharks. *Mol. Biol. Evol.* **42**, https://doi.org/10.1093/molbev/msaf043 (2025).
57. Yamaguchi, K., Koyanagi, M. & Kuraku, S. Visual and nonvisual opsin genes of sharks and other nonosteichthyan vertebrates: Genomic exploration of underwater photoreception. *J. Evol. Biol.* **34**, 968–976 (2021).
58. Hart, N. S. et al. Visual opsin diversity in sharks and rays. *Mol. Biol. Evol.* **37**, 811–827 (2019).
59. Pan, D., Wang, Z., Chen, Y. & Cao, J. Melanopsin-mediated optical entrainment regulates circadian rhythms in vertebrates. *Commun. Biol.* **6**, 1054 (2023).
60. Berson, D. M., Dunn, F. A. & Takao, M. Phototransduction by retinal ganglion cells that set the circadian clock. *Science* **295**, 1070–1073 (2002).
61. Altimus, C. M. et al. Rod photoreceptors drive circadian photoentrainment across a wide range of light intensities. *Nat. Neurosci.* **13**, 1107–1112 (2010).
62. Fisk, A. T., Lydersen, C. & Kovacs, K. M. Archival pop-off tag tracking of Greenland sharks Somniosus microcephalus in the High Arctic waters of Svalbard, Norway. *Mar. Ecol. Prog. Ser.* **468**, 255–265 (2012).
63. Telese, F., Gamliel, A., Skowronska-Krawczyk, D., Garcia-Bassets, I. & Rosenfeld, M. G. "Seq-ing" insights into the epigenetics of neuronal gene regulation. *Neuron* **77**, 606–23 (2013).
64. Solovei, I. et al. Nuclear architecture of rod photoreceptor cells adapts to vision in mammalian evolution. *Cell* **137**, 356–368 (2009).
65. Chao, D. L. & Skowronska-Krawczyk, D. ELOVL2: Not just a biomarker of aging. *Transl. Med. Aging* **4**, 78–80 (2020).
66. Vidal-Vázquez, N. et al. A single-nucleus RNA sequencing atlas of the postnatal retina of the shark Scyliorhinus canicula. *Sci. Data* **12**, 228 (2025).
67. Lewandowski, D. et al. Dynamic lipid turnover in photoreceptors and retinal pigment epithelium throughout life. *Prog. Retin Eye Res* **89**, 101037 (2022).
68. Agbaga, M.-P. et al. Differential composition of DHA and very-long-chain PUFAs in rod and cone photoreceptors. *J. Lipid Res.* **59**, 1586–1596 (2018).
69. Sander, C. L. et al. Nano-scale resolution of native retinal rod disk membranes reveals differences in lipid composition. *J Cell Biol.* **220**, https://doi.org/10.1083/jcb.202101063 (2021).
70. Winnikoff, J. R., Haddock, S. H. D. & Budin, I. Depth- and temperature-specific fatty acid adaptations in ctenophores from extreme habitats. *J Exp Biol.* **224**, https://doi.org/10.1242/jeb.242800 (2021).
71. Dasyani, M. et al. Elovl2 is required for robust visual function in zebrafish. *Cells* **9**, 2583 (2020).
72. Gao, F. et al. Retinal polyunsaturated fatty acid supplementation reverses aging-related vision decline in mice. *Sci. Transl. Med.* **17**, eads5769 (2025).
73. Winnikoff, J. R. & Budin, I. Homeocurvature: a new dimension of membrane adaptation to extreme environments. *Prog. Lipid Res.* **100**, 101355 (2025).
74. Soja-Woźniak, M. et al. Loss of sea ice alters light spectra for aquatic photosynthesis. *Nat. Commun.* **16**, 4059 (2025).
75. Firsanov, D. et al. Evidence for improved DNA repair in long-lived bowhead whale. *Nature* **648**, 717–725 (2025).
76. Bardwell, A. J., Bardwell, L., Tomkinson, A. E. & Friedberg, E. C. Specific cleavage of model recombination and repair intermediates by the Yeast Rad1-Rad10 DNA endonuclease. *Science* **265**, 2082–2085 (1994).
77. Davies, A. A., Friedberg, E. C., Tomkinson, A. E., Wood, R. D. & West, S. C. Role of the Rad1 and Rad10 proteins in nucleotide excision repair and recombination. *J. Biol. Chem.* **270**, 24638–24641 (1995).
78. Radford, S. J., Goley, E., Baxter, K., McMahan, S. & Sekelsky, J. Drosophila ERCC1 is required for a subset of MEI-9-dependent meiotic crossovers. *Genetics* **170**, 1737–45 (2005).
79. Klein Douwel, D. et al. XPF-ERCC1 acts in Unhooking DNA interstrand crosslinks in cooperation with FANCD2 and FANCP/SLX4. *Mol. Cell* **54**, 460–71 (2014).

80. Kikuchi, K. et al. Structure-specific endonucleases Xpf and Mus81 play overlapping but essential roles in DNA repair by homologous recombination. *Cancer Res.* **73**, 4362–4371 (2013).
81. Zaksauskaite, R., Thomas, R. C., van Eeden, F. & El-Khamisy, S. F. Tdp1 protects from topoisomerase 1–mediated chromosomal breaks in adult zebrafish but is dispensable during larval development. *Sci. Adv.* **7**, eabc4165 (2021).
82. Cleaver, J. E., Lam, E. T. & Revet, I. Disorders of nucleotide excision repair: the genetic and molecular basis of heterogeneity. *Nat. Rev. Genet.* **10**, 756–768 (2009).
83. Bishop, S., Francis, M., Duffy, C. & Montgomery, J. Age, growth, maturity, longevity and natural mortality of the shortfin mako shark (Isurus oxyrinchus) in New Zealand waters. *Mar. Freshw. Res.* **57**, 143–154 (2006).
84. Perry, C. T. et al. Comparing length-measurement methods and estimating growth parameters of free-swimming whale sharks (Rhincodon typus) near the South Ari Atoll, Maldives. *Mar. Freshw. Res.* **69**, 1487–1495 (2018).
85. Moreira, I. et al. Growth and maturity of the lesser-spotted dogfish (Linnaeus, 1758) in the southern Portuguese continental coast. *J. Fish. Biol.* **100**, 315–319 (2022).
86. Michael, S. W. Reef sharks and rays of the world. A guide to their identification, behaviour, and ecology. 2009/05/11 ed. Sea challengers. *J. Mar. Biol. Assoc. UK* **73**, 99–102 (1993).
87. Chen, W., Chen, P., Liu, K.-M. & Wang, S.-B. Age and growth estimates of the Whitespotted Bamboo Shark, Chiloscyllium plagiosum, in the Northern Waters of Taiwan. *Zool. Stud.* **46**, 92–102 (2007).
88. Fahmi, W. et al. Age and growth of the tropical oviparous shark, Chiloscyllium punctatum in Indonesian waters. *J. Fish. Biol.* **99**, 921–930 (2021).
89. Cardiff, R. D., Miller, C. H. & Munn, R. J. Manual hematoxylin and eosin staining of mouse tissue sections. *Cold Spring Harb. Protoc.* **2014**, 655–8 (2014).
90. Chen, S., Zhou, Y., Chen, Y. & Gu, J. Fastp: an ultra-fast all-in-one FASTQ preprocessor. *Bioinformatics* **34**, i884–i890 (2018).
91. Simpson, J. T. et al. ABySS: a parallel assembler for short read sequence data. *Genome Res.* **19**, 1117–23 (2009).
92. Simão, F. A., Waterhouse, R. M., Ioannidis, P., Kriventseva, E. V. & Zdobnov, E. M. BUSCO: assessing genome assembly and annotation completeness with single-copy orthologs. *Bioinformatics* **31**, 3210–3212 (2015).
93. Edgar, R. C. MUSCLE: a multiple sequence alignment method with reduced time and space complexity. *BMC Bioinforma.* **5**, 113 (2004).
94. Capella-Gutiérrez, S., Silla-Martínez, J. M. & Gabaldón, T. trimAl: a tool for automated alignment trimming in large-scale phylogenetic analyses. *Bioinformatics* **25**, 1972–3 (2009).
95. Minh, B. Q. et al. IQ-TREE 2: new models and efficient methods for phylogenetic inference in the genomic era. *Mol. Biol. Evol.* **37**, 1530–1534 (2020).
96. Zhang, C., Rabiee, M., Sayyari, E. & Mirarab, S. ASTRAL-III: polynomial time species tree reconstruction from partially resolved gene trees. *BMC Bioinforma.* **19**, 153 (2018).
97. Letunic, I. & Bork, P. Interactive Tree Of Life (iTOL) v5: an online tool for phylogenetic tree display and annotation. *Nucleic Acids Res.* **49**, W293–W296 (2021).
98. Mayeur, H. et al. The Sensory Shark: High-quality Morphological, Genomic and Transcriptomic Data for the Small-spotted Catshark Scyliorhinus Canicula Reveal the Molecular Bases of Sensory Organ Evolution in Jawed Vertebrates. *Mol. Biol. Evol.* **41**, https://doi.org/10.1093/molbev/msae246 (2024).
99. Hara, Y. et al. Shark genomes provide insights into elasmobranch evolution and the origin of vertebrates. *Nat. Ecol. Evol.* **2**, 1761–1771 (2018).
100. Yamaguchi, K. et al. Elasmobranch genome sequencing reveals evolutionary trends of vertebrate karyotype organization. *Genome Res* **33**, 1527–1540 (2023).
101. Stanhope, M. J. et al. Genomes of endangered great hammerhead and shortfin mako sharks reveal historic population declines and high levels of inbreeding in great hammerhead. *iScience* **26**, 105815 (2023).
102. Zhang, Y. et al. The White-Spotted bamboo shark genome reveals chromosome rearrangements and fast-evolving immune genes of cartilaginous fish. *iScience* **23**, 101754 (2020).
103. Kuznetsov, D. et al. OrthoDB v11: annotation of orthologs in the widest sampling of organismal diversity. *Nucleic Acids Res.* **51**, D445–d451 (2023).
104. Gabriel, L. et al. BRAKER3: Fully automated genome annotation using RNA-seq and protein evidence with GeneMark-ETP, AUGUSTUS, and TSEBRA. *Genome Res.* **34**, 769–777 (2024).
105. Sayers, E. W. et al. Database resources of the national center for biotechnology information. *Nucleic Acids Res.* **50**, D20–d26 (2022).
106. Slater, G. S. C. & Birney, E. Automated generation of heuristics for biological sequence comparison. *BMC Bioinforma.* **6**, 31 (2005).
107. Kim, D., Paggi, J. M., Park, C., Bennett, C. & Salzberg, S. L. Graph-based genome alignment and genotyping with HISAT2 and HISAT-genotype. *Nat. Biotechnol.* **37**, 907–915 (2019).
108. Dainat, J. Another Gtf/Gff analysis toolkit (AGAT): resolve interoperability issues and accomplish more with your annotations. In *Plant and Animal Genome XXIX Conference*. (NBS, 2022).
109. Wertheim, J. O., Murrell, B., Smith, M. D., Kosakovsky Pond, S. L. & Scheffler, K. RELAX: detecting relaxed selection in a phylogenetic framework. *Mol. Biol. Evol.* **32**, 820–832 (2014).
110. Smith, M. D. et al. Less is more: an adaptive branch-site random effects model for efficient detection of episodic diversifying selection. *Mol. Biol. Evol.* **32**, 1342–53 (2015).
111. Pond, S. L. K., Frost, S. D. W. & Muse, S. V. HyPhy: hypothesis testing using phylogenies. *Bioinformatics* **21**, 676–679 (2004).
112. Xu, Q. et al. Stress induced aging in mouse eye. *Aging Cell* **21**, e13737 (2022).
113. Gao, F., Tom, E., Lieffrig, S. A., Finnemann, S. C. and Skowronska-Krawczyk, D. A novel quantification method for retinal pigment epithelium phagocytosis using a very-long-chain polyunsaturated fatty acids-based strategy. *Front Mol Neurosci.* **16**, 1279457 (2023).
114. Bligh, E. G. & Dyer, W. J. A rapid method of total lipid extraction and purification. *Can. J. Biochem. Physiol.* **37**, 911–7 (1959).
115. Dobin, A. et al. STAR: ultrafast universal RNA-seq aligner. *Bioinformatics* **29**, 15–21 (2013).
116. Anders, S., Pyl, P. T. & Huber, W. HTSeq-a Python framework to work with high-throughput sequencing data. *Bioinformatics* **31**, 166–9 (2015).
117. R Core Team. R: a language and environment for statistical computing. (R Foundation for Statistical Computing, 2022).

Acknowledgements

We dedicate this article to the memory of our co-author, Prof. John Fleng Steffensen, who sadly passed away before its publication. John was not only an exceptional scientist but also a kind and inspiring collaborator. His pioneering research on Greenland sharks, including the landmark study that first revealed their extraordinary longevity, laid the foundation for our current work. We are deeply grateful for his insight, enthusiasm, and enduring inspiration, and we recognise his lasting contribution to the field. We would like to thank the crew of the RV Porsild as well as the staff at the Arctic Station in Qeqertarsuaq, Greenland for invaluable help fishing for Greenland sharks. We thank David Salom for his technical expertise with the rhodopsin spectral sensitivity experiment. We thank Gulab Zode for generously providing the human corneal samples used in this study. We thank Ghislain Bardout and the Under the Pole team for

kindly providing the photographs in Figure 1a and Figure S1. We acknowledge the staff of the Department of Biosystems Science and Engineering, ETH Zurich for genome and transcriptome sequencing. Figure 1e was created in BioRender [Fogg, L. (2025) https://BioRender.com/ybje926]. All genomic and transcriptomic computations were performed at sciCORE (http://scicore.unibas.ch/), the center of scientific computing at the University of Basel (with support from the Swiss Institute of Bioinformatics). We acknowledge the following funding sources: JFS was supported by the Independent Research Fund Denmark (9040-00303B), the Danish Center for Marine Research (2022-01) and the Carlsberg Foundation (CF20-0519; CF23-1455); WS was supported by the Swiss National Science Foundation and the University of Basel; DSK laboratory was supported by an NIH grant (U01EY034594) and in part by the support to the Gavin Herbert Eye Institute at the University of California, Irvine from an unrestricted grant from Research to Prevent Blindness and from an NIH core grant (P30 EY034070).

Author contributions

Conceptualization: L.F., D.S.K., W.S., J.F.S., R.B., and P.G.B. Methodology: L.F., M.P., E.T., D.S.K., N.B., D.H., A.E.F., C.J.N., and W.S. Investigation: L.F., E.T., W.C., F.G., D.H., A.E.F., C.J.N., D.S.K., A.B., K.F.S., P.G.B., J.F.S., and R.B. Formal analysis: L.F., E.T., W.C., F.G., D.H., A.E.F., C.J.N., and D.S.K. Visualization: L.F., E.T., W.C., F.G., D.H., A.E.F., and D.S.K. Funding acquisition: W.S., D.S.K., and J.F.S. Supervision: L.F., C.J.N., W.S., and D.S.K. Writing – original draft: L.F., E.T., D.S.K., and W.S. Writing – review & editing: L.F., E.T., M.P., W.C., F.G., D.H., A.E.F., N.B., A.B., K.F.S., C.J.N., P.G.B., J.F.S,. R.B., W.S., and D.S.K.

Competing interests

The authors declare no competing interests.

Additional information

Supplementary information The online version contains supplementary material available at https://doi.org/10.1038/s41467-025-67429-6.

Correspondence and requests for materials should be addressed to Lily G. Fogg, Walter Salzburger or Dorota Skowronska-Krawczyk.

Peer review information *Nature Communications* thanks Nathan Hart, Shaun Collin and the other anonymous, reviewer(s) for their contribution to the peer review of this work. A peer review file is available.

Reprints and permissions information is available at http://www.nature.com/reprints

Publisher's note Springer Nature remains neutral with regard to jurisdictional claims in published maps and institutional affiliations.

Open Access This article is licensed under a Creative Commons Attribution-NonCommercial-NoDerivatives 4.0 International License, which permits any non-commercial use, sharing, distribution and reproduction in any medium or format, as long as you give appropriate credit to the original author(s) and the source, provide a link to the Creative Commons licence, and indicate if you modified the licensed material. You do not have permission under this licence to share adapted material derived from this article or parts of it. The images or other third party material in this article are included in the article's Creative Commons licence, unless indicated otherwise in a credit line to the material. If material is not included in the article's Creative Commons licence and your intended use is not permitted by statutory regulation or exceeds the permitted use, you will need to obtain permission directly from the copyright holder. To view a copy of this licence, visit http://creativecommons.org/licenses/by-nc-nd/4.0/.

© The Author(s) 2026